# Ozone sensing study of sprayed β-In2S3 thin films

R. Souissi, N. Bouguila, Marc Bendahan, K. Aguir, T. Fiorido, M. Abderrabba, I. Halidou, A. Labidi

▶ **To cite this version:**

HAL Id: hal-03927840

https://amu.hal.science/hal-03927840

Submitted on 6 Jan 2023

Tunisia, September 28-2021

**Object**: Manuscript submission

**Manuscript title**: Ozone sensing study of sprayed $\beta$-In$_2$S$_3$ thin films

**Authors:** R. Souissi, N. Bouguila, M. Bendahan, K. Aguir, T. Fiorido, M. Abderrabba, I. Halidou[d], A. Labidi

Corresponding author: Riadh Souissi (R. Souissi)

Email : riadhsouissi1@gmail.com

*Dear Editor,*

*We would like to submit the following manuscript "Ozone sensing study of sprayed β-In$_2$S$_3$ thin films". We affirm that the manuscript has been prepared in accordance with journal instructions for contributors and all authors have agreed to be submitted to journal of Alloys and Compounds.*

*Remaining to your disposition for all modifications that you would judge necessary, we ask you to accept, dear Mr, the expression of our better considerations.*

*Best regards,*

*R. Souissi*

$In_2S_3$ material has been eventually used in optoelectronic and photovoltaic. This work reports on the integration of $In_2S_3$ material for use as an ozone sensor. $In_2S_3$ thin films were deposited on $SiO_2$/Si substrates by inexpensive and simple spray pyrolysis technology. Structural, morphological, optical and ozone sensing properties of films have been investigated. We have shown that the sensor shows good reproducibility and it is able to detect an ozone concentration of 40 ppb by increasing resistance 1.5 times. The selectivity study shows that the $In_2S_3$ sensor is highly sensitive to ozone and nitrogen dioxide at 160°C while at 350°C this property is balanced in favor of volatile organic compounds. This work reveals the sensing potential of $In_2S_3$ film deposited by spray pyrolysis route for highly sensitive and ppb-level $O_3$ detection.

# Ozone sensing study of sprayed β-In$_2$S$_3$ thin films

R. Souissi[a,*], N. Bouguila[b], M. Bendahan[c], K. Aguir[c], T. Fiorido[c], M. Abderrabba[a], I. Halidou[d], A. Labidi[e]

[a]*CarthageUniversity, Laboratoire des Matériaux, Molécules et Applications IPEST, BP 51, La Marsa 2070, Tunis, Tunisia.*

[b]*GabèsUniversity, Laboratoire de Physique des Matériaux et des Nanomatériaux Appliquée à l'Environnement, Faculté des Sciences de Gabès, Cité Erriadh, Zrig, 6072 Gabès, Tunisia.*

[c]*Aix Marseille University, Université de Toulon, CNRS, IM2NP, Marseille, France.*

[d]*Département de Physique, Faculté des Sciences et Techniques, Université Abdou Moumouni, BP 10662, Niamey Niger.*

[e]*Department of Physics, College of Science and Art at Ar-Rass, Qassim University, Buraydah 51921, Saudi Arabia.*

## Abstract

In order to integrate new sensitive materials for ozone (O$_3$) detection, In$_2$S$_3$ films were prepared via a facile pyrolysis spray method. Physical properties of the obtained samples were investigated by GIXD, AFM, SEM, EDS, XPS, PL and UV-visible spectroscopy techniques. The sensor shows high sensitivity to ozone and the limit of O$_3$ detection is as low as 40 ppb. The optimal working temperature is found to be 160°C and the detection mechanism is based on dissociative chemisorption. In addition, the gas sensor exhibits acceptable rapidity and good selectivity to O$_3$ at 160°C. This study demonstrates the possibility of producing inexpensive and sensitive ozone gas sensors based on sprayed In$_2$S$_3$ films.

## Keywords

In$_2$S$_3$ film; spray pyrolysis; ozone; gas sensor

*Correspondingauthor: RiadhSouissi (R. Souissi)*

*E-mail: riadhsouissi1@gmail.com*

**I. Introduction**

Ozone ($O_3$) is a naturally occurring gas in our atmosphere. It is an essential constituent of the stratosphere at an altitude of between 15 and 20 km ensuring a primordial role of UV filter. In the troposphere on the surface of our planet, it is a major secondary pollutant resulting from the chemical transformation between nitrogen oxides ($NO_x$) and volatile organic compounds (VOC) under the sunlight during the hot days. Furthermore, ozone is used for drinking water disinfection and has advantages over chlorine which may be carcinogenic [1]. Ozone can also kill pests in foods and has a potential to inactive microbes, bacteria, fungi, and viruses [2]. From an environmental point of view, ozone inhibits the photosynthesis process of certain plants and also contributes to the green house effect [3]. Even at very low concentration, ozone is considered as hazardous air pollutant it is extremely harmful to the lungs, kidneys, brain and eyes [2,3]. According to the recommendation, Mecklenburg County monitoring data show a 2020 ozone compliance value of 67 ppb for each 8 hours [4]. Therefore, it is vital to detect and monitor $O_3$ concentration for the prevention of human health risks. Researchers have tried to detect ozone gas in the air by several methods such as optical ultraviolet absorption and electrochemical methods [5-7]. Metal oxide semiconductors (MOS) such as $Co_3O_4$ [8], $ZnO/SnO_2$ [9], $In_2O_3$ [10], $WO_3$ [11] and $CuAlO_2$ [12] are the most investigated in this field. Indeed, these semiconductors keep a head role because of their high sensitivity, low cost and easy integration. Nevertheless, they continue to suffer from stability problem and high operating temperature. Recently, metal sulfides such as $In_2S_3$[13], $MoS$ [14], $CdS$ and $SnS_2$ [15], have shown competitive sensing properties with respect to their oxides counterparts for nitrogen dioxide ($NO_2$) and volatile organic compounds (VOCs). They reveal an upgrading towards selectivity, stability and the possibility to work at room temperature. They are promising candidates to advance several gas detection applications due to the abundant choice of materials [16]. However, few studies have been devoted to this novel gas sensing

class. In particular and to the best of our knowledge, there is no report on indium sulfide characterization in ozone detection application. This is prompted us to investigate $In_2S_3$ material within the frame work of this goal.

$In_2S_3$ is a group III-VI n-type semiconductor [17]. It is a crystalline compound which exists at atmospheric pressure in three crystallographic forms: $\alpha$-$In_2S_3$ (defect cubic structure), $\beta$-$In_2S_3$ (defect spinel structure obtained in either the expected cubic or tetragonal form), and $\gamma$-$In_2S_3$ (layered hexagonal structure); the $\beta$ phase is the most stable at ambient temperature [18]. Its transmittance is high (70-80%) in the visible and near infrared. Its gap is direct ranging from 2 to 3 eV and its resistivity is quite elevated varying from $10^2$ to $10^6$ $\Omega$.cm [19-21]. $In_2S_3$ is used in several applications such as photodetection [22], photocatalysis [23]. It is also used as contact layer for solar cells [24] and more recently as gas sensor [13]. In fact, we have previously reported the effect of $In_2S_3$ film thickness on VOCs sensing characteristics and we have found that the response was about 10 to 500 ppm ethanol or isopropanol at working temperature of 350°C [25]. In another report, we have shown high sensitivity of $In_2S_3$ material to nitrogen dioxide and with a response of 64 to 5 ppm $NO_2$ at optimal temperature of 200°C [26]. In view of its interesting properties and its important applications, $In_2S_3$films were elaborated by several methods such as Spray Pyrolysis [27,28], Chemical Bath Deposition (CBD) [29,30], Physical Vapor Deposition [31], Ultrasonic Dispersion [32], etc. In this work, we have used Spray Pyrolysis method because it is simple, economical and does not require vacuum. Physical and ozone sensing properties of the prepared films were investigated using different techniques and DC electrical characterization, respectively.

## 2 Experimental procedures

### 2.1 $In_2S_3$ film fabrication

The Chemical Spray Pyrolysis (CSP) technique was used to grow indium sulfide ($In_2S_3$) thin films. $InCl_3$ and $SC(NH_2)_2$ were used as precursors in aqueous solution. The concentration of

$InCl_3$ and $SC(NH_2)_2$ precursors is $10^{-2}$ mol.$L^{-1}$ and the molar ratio S/In in solution was set at 2. The solution and nitrogen carrier gas flow rates were fixed at 2 mL.$min^{-1}$ and 6 L.$min^{-1}$, respectively. The mixture fluid was sprayed during 2 min on $Si/SiO_2$ substrate heated at 350°C. Electrical contact was assured by interdigitated microelectrode array composed of alternating a total of 30 platinum fingers deposited by sputtering on $4\times4$ $mm^2$ substrate surface as shown in **Fig. 1(a)**.

## 2.2 Characterization techniques

The crystalline structure of the obtained films was investigated by Grazing Incidence X-ray Diffraction (GIXD), using a diffractometer with monochromatic Cu-$K\alpha_1$ radiation ($\lambda = 1.5406$ Å). The film morphological characterizations were performed using an XE-100 atomic force microscope (Park Systems Corporation) in non-contact mode (NC-AFM) and by a scanning electron microscope (SEM) using a Zeiss FE-SEM ULTRA Plus microscope which is endowed with an electron dispersive spectrometer (EDS) for chemical composition determination. The surface contents were also analyzed by X-ray photoelectron spectroscopy (XPS, ESCALAB 250Xi, Thermo Scientific, USA). Transmittance and reflectance of the films have been investigated using a Shimadzu UV-3101 PC spectrophotometer with wavelength range between 250 nm to 2400 nm. Photoluminescence (PL) measurements were performed at room temperature using Perklia Elmer LS55 Fluorescence spectrometer with laser excitation wavelength of 400 nm.

## 2.3 Experimental set-up for ozone detection

The ozone sensing properties of the $In_2S_3$ film were investigated using the experimental set-up shown in **Fig. 1(b)**. The sample was placed in the test chamber. After a 3 min exposure of $In_2S_3$ film to ozone, pure air was conveyed directly to the test chamber and the flow rate was maintained by a mass flow controller at 0.4 L.$min^{-1}$. The sample was polarized at 0.5 V and exposed by an ozone calibration source at various concentrations. Current intensity through

the sample was measured using Keithley-2550 source/nano-ammeter, interfaced to a computer for data acquisition. The operating temperature was varied in the range 100-300°C and directed by an IPS-405 DC voltage source.

In order to evaluate the response of the $In_2S_3$ sensor, we have used formula (1) and (2) for oxidant and reducing gases, respectively [33,34]:

$$Response = R_{gas}/R_{air} \tag{1}$$

$$Response = R_{air}/R_{gas} \tag{2}$$

Where, $R_{air}$ and $R_{gas}$ are the sensor resistance value under dry air and target gas, respectively. Likewise, sensitivity is defined by Eq. (3) [35]:

$$S = \frac{\partial Response)}{\partial C_{gas}} \tag{3}$$

Where, $C_{gas}$ denotes the concentration of target gas. The slope of the fitting line between sensing response and concentration represents the sensitivity ($S$) of the tested sensors.

## 3. Results and discussion

### 3.1 Characterization

### 3.1.1 Sample microstructure and morphology

In order to study $In_2S_3$ film microstructure, Grazing Incidence X-ray Diffraction was carried out. Such technique allows the known of the in-depth distribution of different crystalline phases composing the surface of a compound by griping quite weak X-ray incidence angle to limit penetration depth. The X-ray diffraction patterns of the $In_2S_3$ film for three X-ray incidence angles were shown in **Fig. 2(a)**. It is clear that peaks intensities increase by rising incidence angle from 0.1 degree to 0.3 degree. The obtained peaks confirm the arrangement of $In_2S_3$ film under simple cubic structure with reticular planes (111), (220), (311), (400), (331), (511), (440), (531) and (533) which correspond to the standard JCPDS data card n°32-0456. The appearance of several diffraction peaks reveals that the material is polycrystalline. The presence of bumps at low angles in the diffractograms can be credited to the amorphous $SiO_2$

layer on top of the Si substrate. Moreover, no diffraction peaks of any other secondary phase could be spotted, which shows the purity of the specimen.

The average size D of the crystallites and the lattice micro-strain $\varepsilon$ of the $In_2S_3$ particles were evaluated using the Williamson-Hall (WH) method based on the equation (4) [36]:

$$\beta cos\theta = \frac{k\lambda}{D} + 4\varepsilon \, sin\theta \tag{4}$$

Where $\theta$ is the Bragg angle in radians, $\beta$ is the full-width at half maximum (FWHM), $k$ is a constant (equal to 0.9), $\varepsilon$ is the strain and $\lambda$ is the X-ray wavelength.

We used a Lorentzian fit, so the full width at half maximum is determined by:

$$\beta = \beta_e - \beta_0 \tag{5}$$

With $\beta_e$ the experimental width and $\beta_0$ is the instrumental width ($\beta_0 = 1.5.10^{-3}$ rad).

Williamson-Hall plot matching the X-ray pattern obtained under 0.3 degree of $In_2S_3$ film is shown in Fig. 2(b).The curve of $\beta cos\theta$ along the y-axis versus $4sin\theta$ along the x-axis gives the strain through the slope of the graph and the displayed $\varepsilon$ value is $1.4 \, 10^{-3}$. Such positive value indicates the existence of a small micro-tensile in the crystalline network due to crystal imperfection and distortion. The particles size can be estimated from the y-intercept and the obtained $D$ value is 39 nm.

The surface morphology was studied by NC-AFM technique. **Fig. 3(a) and (b)** show 2D and 3D topographic images ($2\times2\mu m^2$) of $In_2S_3$ film. They reveal that the substrate surface is entirely covered with grains of different sizes. As can be seen, $In_2S_3$ film has a prism-like morphology, the 3-D image indicates a columnar structure owing to the low mobility of the atoms deposited on the substrate. The layer is dense and have rough surface. The RMS roughness (Rq) is estimated to be in the order of 10 nm.

SEM micrograph of the $In_2S_3$ thin film sprayed on glass substrates are shown in **Fig. 3(c)**. It is observed that the $In_2S_3$ film has granular surface morphology with individual grains and voids between them. The granules have various scales. Fig. 3(d) shows the grain size distribution in

the form of the histogram with random distribution for the $In_2S_3$ nanostructured thin film. The mean grain size obtained from the histogram was just about 28 nm. Comparing with the grain size determined by X-ray measurements using the Williamson-Hall method, it can be concluded that each grain is made up of a mono crystallite.

### 3.1.2 Chemical analysis

In order to determine the atomic concentration of constituent elements, quantitative analysis of the $In_2S_3$ film deposited on glass substrate was performed using energy dispersive spectroscopy (EDS). **Fig. 4** shows EDS spectra registered for $In_2S_3$ film and glass substrate.

The EDS spectrum of $In_2S_3$ film corroborates the existence of In and S elements in the layer. The atomic concentrations of constituent elements are given in **Table 1**. It can be noted that the S/In molar ratio in the film is 1.7. The Cl peak originates from the $InCl_3$ precursor. We also see the presence of a variety of elements such as Si, O, Na and Ca which are originated from the glass substrate as shown in **Fig. 4(b)**.

In the same way and in order to verify the surface chemical elemental composition of the sample, X-ray photoelectron spectroscopy (XPS) analysis was performed and the comprehensive information is illustrated in **Fig. 5**. All peaks are accurate and well defined. The kinetic energy for In MNN is about 975 eV (**Fig. 5(a)**), which corresponds to that of $In_2S_3$. **Fig. 5(a)** also shows that XPS spectrum includes C 1s, S 2p, In 4d, and In 3d core levels characteristic of carbon, sulphur and indium elements, respectively. The peak located at about 285 eV is attributed to the C 1s of absorbed molecule $CO_2$ in the layer from air [22]. Moreover, The XPS analysis indicates that the film predominantly consists of sulphur and indium atoms. **Fig. 5(b)** shows the S2p peaks. The binding energies 161.4 eV and 162.9 eV, assigned respectively to S $2p_{3/2}$ and S $2p_{1/2}$ peaks, correspond to sulfurized phases. As observed in **Fig. 5(c)**, the In $3d_{5/2}$ core shell with energy 444.9 eV and In $3d_{3/2}$ at 452.9 eV correspond to the elements present in $In_2S_3$ compound [37,38]. We do not see any asymmetry

of In $3d_{3/2}$ and In $3d_{1/2}$ peaks. These values are in good agreement with the values reported in the literature [38]. In addition, we see in **Fig. 5(d)** that the XPS spectrum contains O 1s core levels which can be split into three peaks. The peak with the lowest bending energy, situated in the energy range 529.8 eV-530.5 eV, is ascribed to lattice oxygen for indium oxides $In_2O_3$ [39]. The O 1s peak at about 531.8 eV is associated with oxygen vacancy and the last peak at 232.4 eV is assigned to adsorbed oxygen [39].

### 3.1.3 UV-visible and PL characterization

In order to investigate the $In_2S_3$ optical properties, transmittance (*T*) and reflectance (*R*) spectra are recorded in the wavelength domain 300-2400 nm (**inset of Fig. 6(a)**). The transmittance is more than 70% in the visible and near infrared region whereas reflectance is about 20%. The evolution of the transmittance first derivative (*dT/dλ*) versus wavelength (*λ*) is illustrated in **Fig. 6(a).** The derivative has its maximum value at a wavelength of 420 nm. The band gap energy is initially deduced from the maximum of (*dT/dλ*) and estimated to be equal to 2.9 eV [40].

In order to precisely calculate the value of the optical band gap energy as well as the nature of the transition occurring, we have tracked a method previously used by Bhattacharyya et al. [41] and Barreau et al. [42]. The sample absorption coefficient (α) has been estimated using the following formula [42]:

$$\alpha = \frac{1}{t}\log(\frac{(1-R)^2}{T}) \tag{6}$$

Where *t* = 200 nm is the layer thickness while *R* and *T* are respectively the reflectance and the transmittance.

The absorption coefficient α is related to incident photon energy (hν) in the mean absorption edge by Tauc formula [43]:

$$\alpha = A\,(h\nu - E_g)^n/h\nu \tag{7}$$

Where *A* and *n* are constants and $E_g$ is the band gap energy.

8

The exponent n can take the value of 0.5, 2, 1.5 or 3 for allowed direct, allowed indirect, forbidden direct or forbidden indirect transition, respectively. In order to determine the n value, the following relation can be deduced from Eq. (7):

$$\ln(\alpha h\nu) = \ln(A) + n\ln(h\nu - E_g) \tag{8}$$

The plot of $ln(\alpha h\nu)$ versus $ln(h\nu\text{-}E_g)$, with $E_g$ = 2.9eV, is shown in **Fig. 6(b)**. The deduced curve slope is about 0.5 which is assigned to n value. Therefore, the transition occurring has a direct allowed nature. Relation (7) can consequently be rewritten as follow:

$$\alpha = A\,(h\nu - E_g)^{1/2}/h\nu \tag{9}$$

The value of $E_g$ (2.9 eV) estimated above is not sufficiently precise. A more accurate value can be determined by extrapolating to 0 the linear region of the curve $(\alpha h\nu)^2$ as a function of photon energy (hν), depicted in **Fig. 6(c).** The obtained $E_g$ value is 2.82 eV, this later is in agreement with reported energy band gap in literature [44-46].

Likewise **Fig. 6(d)** exhibits photoluminescence (PL) spectrum of $In_2S_3$ thin film for 400 nm excitation wavelength at room temperature. The results of the adjustment used to reveal the different emissions are also demonstrated. Three peaks at 2.35 eV (527nm), 2.22 eV (558 nm) and 1.83 eV (675 nm) are fitted using Gaussian functions. These peaks reveal the presence of trap states associated with defects in the crystal structure. The green luminescence at 2.35 eV (high intensity) can be attributed to the transition between the sulfur vacancy donor (Sv) level (located 0.48eV below the conduction band) and the valence band [47]. The luminescence at 2.22 eV (medium intensity) and the red luminescence at 1.83 eV (low intensity) can be attributed to transitions between donor and acceptor levels [48,49].

**3.2 Ozone sensing**

**3.2.1. Ozone test and sensing mechanism**

In order to test the sensitivity of $In_2S_3$ material to ozone, the sample was introduced into a test chamber and exposed for 3 min to 400 ppb of ozone followed by an injection of dry air for

approximately 10 min. The working temperature was maintained at 200°C. **Fig. 7(a)** shows the change in resistance of In$_2$S$_3$ layer versus time. We can note that the resistance increases by ozone injection and decreases following its evacuation. This behavior is due to an adsorption/desorption phenomenon of an oxidizing gas on the surface of an n-type semiconductor and suggests the sensitivity of In$_2$S$_3$ material to ozone gas.

Among the different adsorption mechanisms, Wolkenstein's adsorption model [50] seems the most suitable for the case of semiconductor materials. Strong chemisorption occurs when an electron of the conduction band is transferred from the semiconductor of the adsorbed species. The binding energy of the adsorbate increases. This process involves the creation of a negative surface charge and a surface potential barrier induced by chemisorption. This model naturally introduces the reciprocal interactions between the adsorbent and the adsorbate. The adsorption can be dissociative or non-dissociative. For triatomic gases such as ozone ($O_3$), only dissociative adsorption is considered at the working temperature [51,52]. In order to understand the ozone detection mechanism of In$_2$S$_3$ layer, sample resistance measurements were performed with 400 ppb ozone at working temperature in the range 125-300°C. **Fig.7(b)** illustrates the dynamic recording of film resistance during pressure cycles performed at different operating temperatures. It can be noted that the base line (resistance of the sensor in dry air) diminishes from 3300 kΩ to 14.2 kΩ by rising temperature. Such evolution reflects the semiconductor behavior of the material.  Likewise, sensing response has been affected. **Fig.7(c)** depicted the evolution of ozone response versus temperature. It can be seen that the response increases up to 5 times at 160°C and then decreases. Such behavior could be interpreted as a competition between adsorption and desorption rates as given by the Lenard-Jones equation [52]:

$$\frac{d\theta}{dt} = k_{ads}e^{-\frac{E_A}{kT}} - k_{des}\theta e^{-\frac{(E_A + H_c\Box em)}{kT}}$$

(10)

Where $\theta$ is the fraction of presented surface sites covered, $k_{ads}$ and $k_{des}$ are respectively the rate constants for adsorption and desorption reactions, $E_A$ the activation energy of chemisorption, and $H_{chem}$ the heat of chemisorption.

The competition between adsorption and desorption rates leads to maximum response of the sensor at 160°C. The curve slope inversion at this temperature implies a modification in detection mechanism. As known, $O_3$ molecules can only be adsorbed in centers free of oxygen ions. In this regard, we have studied oxygen adsorption by In$_2$S$_3$ layer versus operating temperature. A second In$_2$S$_3$ sample was exposed to dry air through 5 min altered by pure nitrogen during 15 min. The working temperature was varied in the range 150-400°C. The obtained results are illustrated by **Fig. 7(d)** [25]. We have defined the oxygen sensing response as follow:

$$Response\ (O_2) = R_{air}/R_{nitrogen} \tag{11}$$

Where, R$_{air}$ and R$_{nitrogen}$ represent the sensor resistance value in air and in nitrogen atmospheres, respectively.
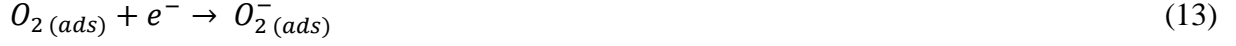
The evolution of oxygen response versus operating temperature is reported in **Fig. 7(c)**. We can note that oxygen adsorption begins above 150°C, reaches saturation at 350°C and then decreases by increasing temperature.

As consequence, we discern two areas:

• T < 160°C: in this domain, the temperature raise induces electrons transitions from donor levels corresponding to sulfur vacancies and interstitial indium to conduction band [53]. This leads to an increase in free electrons concentration and favorites the dissociative chemisorption of ozone molecules as shown by Eq. (12) [54]:

$$O_{3\ (ads)} + e^- \rightarrow O_2 + O^-_{(ads)} \tag{12}$$

• T > 160°C: here, ionization of oxygen coming from air into $O_2^-$, $O^-$ and $O^{2-}$ ions is added to ozone chimisorption as illustrated in **Fig. 7(c)** by the plots of $R_{ozone}/R_{air}$ and $R_{air}/R_{nitrogen}$ versus operating temperature. The corresponding chemical reactions are [26,54]:

$$O_{2\,(ads)} + e^- \rightarrow O_{2\,(ads)}^- \tag{13}$$

$$O_{2\,(ads)} + 2\,e^- \rightarrow 2\,O_{(ads)}^- \tag{14}$$

$$O_{2\,(ads)} + 4\,e^- \rightarrow 2\,O_{(ads)}^{2-} \tag{15}$$

These reactions do not have the same probability of existence but compete with ozone reduction. Raising the temperature above 160°C facilitates the trap of free electrons by highly electronegative oxygen molecules. As a result, the reduction of oxygen intensifies in favor of that of ozone and the transfer of electrons from the In$_2$S$_3$ layer to $O_3$ molecules becomes difficult. Therefore, the response of ozone sensor decreases.

In the other side, when dry air is injected in the test chamber, ozone vapor desorbs from the sensor surface as follow [54]:

$$O_{2\,(ads)} + O^- \rightarrow O_{3(des)} + e^- \tag{16}$$

As a result, the depletion layer is reduced, the liberated electrons return to the conduction band, the concentration of majority carriers increases and the resistance of the material decreases.

### 3.2.2 Ozone sensing properties

**Fig. 8(a)** shows the dynamic changes in resistance of In$_2$S$_3$ film when exposed to ozone as a function of the concentration in the range 40-400 ppb at 160°C working temperature. It is clear that the sensor is able to detect an ozone concentration of approximately 40 ppb. We can note an improvement in the steady state as the gas concentration increases. **Fig. 8(b)** reveals that response rises from 1.5 to 5 times by varying the ozone concentration from 40 ppb to 400 ppb. The film sensitivity, estimated from the slope of the linear adjustment of the response,

12

attains a value of about 0.9 ppb$^{-1}$. Therefore, an In$_2$S$_3$ based sensor is favorable for practical application.

Sensor rapidity can be defined in terms of response and recovery times ($\tau_{rep}$ and $\tau_{rec}$, respectively). The response time is defined as the time necessary for the sensor to achieve 90% of the sensor response, and the recovery time as that required to attain 10% of the initial resistance baseline after the target gas has been purged [55]. From **Fig. 8(a),** we can notice that the duration of the return to the base line increases with the ozone concentration. **Fig. 8(c)** illustrates the evolution of the response and recovery times versus ozone concentration at a working temperature of 160°C. It can be seen that response time decreases from 2.45 min to 2.06 min and the recovery time increases from 6.90 min to 8.53 min by increasing ozone concentration from 40 ppb to 400 ppb. In fact, this is related to the rates of chemical reactions at the surface of the semiconductor. Increasing the adsorbate concentration accelerates the adsorption kinetics while desorption becomes more and more difficult.

In the other side, **Fig. 8(d)** shows the changes in resistance of the In$_2$S$_3$ sensor during the cyclic detection of 125 ppb of ozone at 160°C. The recorded signal shows good response repeatability, reversibility and baseline stability.

In order to investigate the In$_2$S$_3$ sensor selectivity, the sample was tested to 0.25 ppm oxidant gases and 500 ppm volatile organic compounds at two working temperature of 160°C and 350°C as shown in **Fig. 9**. This study reveals that the In$_2$S$_3$ sensor is highly sensitive to ozone and nitrogen dioxide at 160°C while at 350°C this property is balanced in favor of volatile organic compounds. Such evolution can be explained by the detection mechanism monitored by air oxygen adsorption as explained in the previous paragraph. In fact, oxygen ionization above 160°C inhibits $O_3$ and $NO_2$ adsorption but facilities VOCs oxidation by oxygen ions $O_2^-$, $O^-$ and mainly $O^{2-}$ [25]. It should be noted that the response to ozone and nitrogen dioxide is in the same order. This generates the selectivity problem of oxidizing gases. However, it is

possible to examine the dissimilar dynamic responses using a mathematical technique called principal component analysis (PCA) [56]. This investigation is planned for a future work.

A comparison of the performance of $In_2S_3$ developed sensor with that of recently published sensors is reported in **Table 2**. The results in the present work reveal that the detection of ozone by $In_2S_3$ sensor is quite real. In addition, its manufacture by the simple and economic spray pyrolysis method shows that it is competitive with other recently published sensor results.

**Conclusion**

We have deposited $In_2S_3$ layers on $SiO_2/Si$ substrates with inter-digitized platinum electrodes using spray pyrolysis technique. GIXD analysis shows the formation of polycrystalline cubic $\beta$-$In_2S_3$ phase. The XPS measurements indicate that the material is pure. Optical investigation reveals that the layer transmittance is in the range 70-80% in the visible and near infrared region. The band gap is direct and its energy is estimated to 2.82 eV. Morphological study demonstrates that the layer is well covered, dense and has rough surface. The average grain size is found to be in order of 28 nm. Such results are related with the layer best sensing properties. The $O_3$ sensing response versus operating temperature is in concordance with Lennard-Jones law and the optimal working temperature is around 160°C. The sensor shows good reproducibility and it is able to detect an ozone concentration of 40 ppb by increasing resistance 1.5 times. The selectivity study shows that the $In_2S_3$ sensor is highly sensitive to ozone and nitrogen dioxide at 160°C while at 350°C this property is balanced in favor of volatile organic compounds. This work reveals the sensing potential of $In_2S_3$ film deposited by spray pyrolysis route for highly sensitive and ppb-level $O_3$ detection.

**Data availability statement**

The data that support the findings of this study are available from the corresponding author upon reasonable request.

**Conflicts of interest**

There are no conflicts to declare.

**References**

[1] F.S-S. Chien, C-R. Wang, Y-L. Chana, H-L. Linb, M-H. Chenb, R-J. Wub, Fast-response ozone sensor with ZnO nanorods grown by chemical vapor deposition, Sens. Actuators B 144 (2010) 120.

[2] Z. Zhu, J-L. Chang, R-J. Wu, Fast ozone detection by using a core-shell Au@TiO$_2$ sensor at room temperature, Sens. Actuators B 214 (2015) 56.

[3] Z. Zhu, J-L. Chang, C-H. Wu, T-L. Chou, R-J. Wu, Promotion effect of silver on Indium(III) oxide for detecting trace amounts of ozone, Sens. Actuators B 232 (2016) 442.

[4] USEPA: Criteria Air Pollutants, (2020) Available at https://www.epa.gov/criteriaairpollutants.

[5] S.Addanki, J. Jayachandiran, K. Pandian, D. Nedumaran, Development of optical sensors for the quantitative detection of ozone using gold and silver thin film nanoislands, Sens. Actuators B 210 (2015) 17.

[6] J.J. Huntzicker, R.L. Johnson, Investigation of an ambient interference in the measurement of ozone by ultraviolet absorption photometry, Environ.Sci. Technol. 13, 11 (1979) 1414.

[7] X. Pang, M.D. Shaw, A.C. Lewis, L.J. Carpenter, T. Batchellier, Electrochemical ozone sensors: A miniaturised alternative for ozone measurements in laboratory experiments and air-quality monitoring, Sens. Actuators B 240 (2017) 829.

[8] L. Liu, T. Li, Z. Yi, F. Chi, Z. Lin, X. Zhang, K. Xu, Conductometric ozone sensor based on mesoporous ultrafine Co$_3$O$_4$nanobricks, Sens. Actuators B 297 (2019) 126815.

[9] L.F. da Silva,J.-C M'Peko,A.C. Catto, S. Bernardini, V.R. Mastelaro,K. Aguir,C. Ribeiro, E. Longo, UV-enhanced Ozone Gas Sensing Response of ZnO-SnO$_2$Heterojunctions at Room Temperature, Sens. Actuators B 240 (2017) 573.

[10] M. Ivanovskaya, A. Gurlo, P. Bogdanov, Mechanism of O$_3$ and NO$_2$ detection and selectivity of In$_2$O$_3$ sensors, Sens. Actuators B 77 (2001) 264.

[11] M. Bendahan, R. Boulmani, J. Seguin, K. Aguir, Characterization of ozone sensors based on $WO_3$ reactively sputtered films: influence of $O_2$ concentration in the sputtering gas, and working temperature, Sens. Actuators B 100 (2004) 320.

[12] S. Thirumalairajan, V.R. Mastelaro, C.A. EscanhoelaJr,In-Depth understanding of the relation between $CuAlO_2$ particle size and morphology for ozone gas sensor detection at a nanoscale level, ACS Appl. Mater. Interfaces 6 (2014) 21739.

[13] R. Souissi, N. Bouguila, A. Labidi, Ethanol sensing properties of sprayed $\beta$-$In_2S_3$ thin films, Sens. Actuators B 261 (2018) 522.

[14] Y. Zhou, C. Zou, X. Lin, Y. Guo, UV light activated $NO_2$ gas sensing based on Au nanoparticles decorated few-layer $MoS_2$ thin film at room temperature, Appl. Phys. Lett. 113 (2018) 082103.

[15] V. Guidi, B. Fabbri, A. Gaiardo, S. Gherardi, A. Giberti, C. Malagù, G.Zonta, P. Bellutti, Metal sulfides as a new class of sensing materials, Procedia Engineering 120 (2015) 138.

[16] H. Tang, L. Sacco, S. Vollebregt, H. Ye, X. Fan, G. Zhang, Recent advances in 2D/nanostructured metal sulfides-based gas sensors: mechanisms, applications, and perspectives, J. Mater. Chem. A (2020), DOI: 10.1039/D0TA08190F.

[17] N. Naghavi, R. Henriquez, V. Latev, D. Lincot, Growth studies and characterisation of $In_2S_3$ thin films deposited by atomic layer deposition (ALD),Appl. Surf. Sci. 222 (2004) 65.

[18] R. Diehl, R. Nitsche, Vapor growth of three $In_2S_3$ modifications by iodine transport, J. Cryst. Growth 28 (1975) 306.

[19] W.T. Kim, C.D. Kim, Optical energy gaps of $\beta$-$In_2S_3$ thin films grown by spray pyrolysis, J. Appl. Phys. 60 (1986) 2631.

[20] A. Timoumi, H. Bouzouita, B. Rezig, Optical constants of Na-$In_2S_3$ thin films prepared by vacuum thermal evaporation technique, Thin Solid Films 519 (2011) 7615.

[21] N. Revathi, P. Prathap, K.T. Ramackichna Reddy, Thickness dependent physical properties of close space evaporated $In_2S_3$ films, Solide State Sciences 11 (2009) 1288.

[22] B. Hemanth Kumar, M.C. Santhosh Kumar, Indium sulfide based metal-semiconductor-metal ultraviolet-visiblephotodetector, Sens. Actuators A 299 (2019) 111643.

[23] Li Z, Zhou Z, Ma J, Li Y, Peng W, Zhang G, Zhang F, Fan X, Hierarchical photocatalyst of $In_2S_3$ on exfoliated $MoS_2$nanosheets for enhanced visible-light-driven Aza-Henry reaction, Applied Catalysis B: Environmental 237 (2018) 288.

[24] S. Siol, T.P. Dhakal, G.S. Gudavalli, P.P. Rajbhandari, C. DeHart, L. Baranowski, A. Zakutayev, Combinatorial reactive sputtering of $In_2S_3$ as an alternative contact layer for thin film solar cells, ACS Appl. Mater. Interfaces 8, 22 (2016) 14004.

[25] R. Souissi, N. Bouguila, B. Bouricha, C. Vàzquez-Vàzquez, M. Bendahan, A. Labidi, Thickness effect on VOC sensing properties of sprayed $In_2S_3$ films, RSC Adv. 10 (2020) 18841.

[26]R. Souissi, N. Bouguila, M. Bendahan, T. Fiorido, K. Aguir, M. Kraini, C. Vázquez-Vázquez, A.Labidi, Highly sensitive nitrogen dioxide gas sensors based on sprayed β-$In_2S_3$ film, Sens. Actuators B 319 (2020) 128280.

[27] Raid A. Ismail, Nadir F. Habubi, Mahmood M. Abbod, Preparation of high-sensitivity $In_2S_3$/Si hetero junction photodetector by chemical spray pyrolysis, Opt. Quant. Electron 48 (2016) 455.

[28] T. T. John, M. Mathew, C. S. Kartha, K. P. Vijayakumar, T. Abe, and Y. Kashiwaba, $CuInS_2$/$In_2S_3$ thin film solar cell using spray pyrolysis technique having 9.5 % efficiency, Solar Energy Materials and Solar Cells 89 (2005) 27.

[29] M. Kilani, C. Guasch, M. Castagne, N.K. Turki, Structural, optical, and electrical properties of $In_2S_3$:Sn thin films grown by chemical bath deposition on Pyrex, J. Mater. Sci. 47 (2012) 3198.

[30] A. Akkari, C. Guasch, M. Castagne, N.K. Turki, Optical study of zinc blend SnS and cubic In$_2$S$_3$:Al thin films prepared by chemical bath deposition, J. Mater. Sci. 46 (2011) 6285.

[31] S. Rasool, G. Phaneendra Reddy, K. T. Ramakrishna Reddy, M. Tivanov, V. F. Gremenok, Effect of substrate temperature on structural and optical properties of In$_2$S$_3$ thin films grown by thermal evaporation, Materials today Proceeding 4 (2017) 12491.

[32] Z. Li, X. Tao, Z. Wu, P. Zhang, Z. Zhang, Preparation of In$_2$S$_3$ nanoparticle by ultrasonic dispersion and its tribology property, Ultrason Sonochemistry 16 (2009) 221.

[33] K. Schneider, W. Maziarz, V$_2$O$_5$ Thin Films as Nitrogen Dioxide Sensors, Sensors 18 (2018) 4177.

[34] B. Lawson, K. Aguir, T. Fiorido, V. Martini-Laithier, R. Bouchakour, S. Burtey, Ch. Reynard-Carette, M. Bendahan, Skin alcohol perspiration measurements using MOX sensors, Sens. Actuators B. Chemical 280 (2019) 306.

[35] Y. Zhou, G. Liu, X. Zhu, Y. Guo, Ultrasensitive NO$_2$ gas sensing based on rGO/MoS$_2$nanocomposite film at low temperature, Sens. Actuators B 251 (2017) 280.

[36] D. Nath, F. Singh, R. Das, X-ray diffraction analysis by Williamson-Hall, Halder-Wagner and size-strain plot methods of CdSe nanoparticles- a comparative study, Materials Chemistry and Physics 239 (2020) 122021.

[37] X. Fu , X. Wang, Z. Chen, Z. Zhang, Z. Li, D.Y.C. Leung, L. Wu, X. Fu, Photocatalytic performance of tetragonal and cubic b-In$_2$S$_3$ for the water splitting, under visible light irradiation, Applied Catalysis B: Environmental 95 (2010) 393.

[38] M. Mathew, M. Gopinath, C.S. Kartha, K.P. Vijayakumar, Y. Kashiwaba, T. Abe,Tin doping in spray pyrolysed indium sulfide thin films for solar cell applications, Sol. Energy 84 (2010) 888.

[39] N. Reddy, C.V. Reddy, M. Cho, J. Shim, D. Kim, Structural, optical and XPS study of thermal evaporated $In_2O_3$ thin films, Mater. Res. Express 4 (2017) 086406.

[40] M. Benamara, J. Massoudi, H. Dahman, E. Dhahri, L. El Mir, A. Ly, M. Debliquy, D. Lahem, High response to sub‑ppm level of $NO_2$ with 50%RH of ZnO sensor obtained by an auto‑combustion method, Journal of Materials Science: Materials in Electronics 31 (2020) 14249.

[41] D. Bhattacharyya, S. Chaudhuri, A.K. Pal, Band gap and optical transitions in thin films from reflectance measurements, Vacuuum 43 (4) (1992) 313.

[42] N. Barreau, J.C. Bernede, S. Marsillac, Study of the new b-In2S3 containing Na thin films. Part II: Optical and electrical characterization of thin films, Journal of Crystal Growth 241 (2002) 51.

[43] J.I. Pankove, Optical Processes in Semiconductors, Prentice-Hall, Englewood Cliffs, NJ, 1971.

[44] N. Bouguila, M. Kraini, I. Halidou, E. Lacaze, H. Bouchriha, H. Bouzouita, Thickness effect on properties of sprayed $In_2S_3$ films for Photovoltaic Applications, J. Electron. Mater.45 (2016) 829.

[45] N. Barreau, Indium sulfide and relatives in the world of photovoltaics, Solar Energy 83 (2009) 363.

[46] T. Schulmeyer, A. Klein, R. Kneiese, M. Powalla, Band offset at the $CuGaSe_2 / In_2S_3$ heterointerface, Appl. Phys. Lett. 85 (2004) 961.

[47] P.E. Rodriguez-Hernandez, F. DE Moure-Flores, A. Guillencervantes, E. Campos-Gonzalez, J. Santos-Cruz, S.A. Mayenhernandez, J.S. Arias-Ceron, M. DELA L. Olvera, O. Zelayaangel, G. Contreras-Puente, Phsical properties of $In_2S_3$ thin films grown chemical bath deposition at different temperatures, Chalcogenide Letters Vol. 13, No. 8 (2016) 389.

[48] R. Jayakrishnan, T. T. John, C.S. Kartha, K.P. Vijayakumar, T. Abe, Y. Kashiwaba, Defect analysis of sprayed β-In2S3 thin films using photoluminescence studies, Semicond. Sci. Technol.20 (2005) 1162.

[49] R. Jayakrishnan, Photoluminescence in spray pyrolysis deposited b-In$_2$S$_3$thin films, J. Electron.Mater.47 (4) (2018) 2249.

[50] A. Rothschild, Y. Komem, Numerical computation of chemisorption isotherms for device modeling of semiconductor gas sensors, Sens. Actuators B 93 (2003) 362.

[51] H. Ouali, C. Lambert-Mauriat, L. Raymond, A. Labidi, Mechanism of O$_3$sensing on Cu$_2$O (111) surface: First principle calculations, Appl. Surf. Sci. 351 (2015) 840.

[52] J.M. Madou, S.R. Morrison, Chemical Sensing with Solid State Devices, Academic Press, 1989, Chapters 3 and 12, ISBN 0-12-464965-3.

[53] R.R. Pai, T.T. John, Y. Kashiwaba, T. Abe, K.P. Vijayakomar, C.S. Kartha, Defect characterization of spray pyrolised β-In$_2$S$_3$ thin film using Thermally Stimulated Current measurements,J. Mat. Sci. 40 (2005) 741.

[54]N. Sui, P. Zhang, T. Zhou, T. Zhang, Selective ppb-level ozone gas sensor based on hierarchical branch-like In$_2$O$_3$ nanostructure, Sens. Actuators B 336 (2021) 129612.

[55] F.E. Annanouch, G. Bouchet, P. Perrier, N. Morati, C. Reynard-Carette, K. Aguir, V. Martini-Laithier, M. Bendahan, Hydrodynamic evaluation of gas testing chamber: Simulation, experiment, Sens. Actuators B 290 (2019) 598.

[56] X. Vanden Eynde, P. Bertrand, ToF-SIMS quantification of polystyrene spectra based on principal component analysis (PCA), Surface and Interface Analysis 25 (1997) 878.

[57] N. Joshi, L.F. da Silva, H.S. Jadhav, F.M. Shimizu, P.H. Suman, J.-C. M'Peko, M.O. Orlandi, J.G. Seo, V.R. Mastelaro, O.N. Oliveira, Yolk-shelled ZnCo$_2$O$_4$ microspheres: surface properties and gas sensing application, Sens. Actuators B 257 (2018) 906.

[58] Y.J. Onofre, A.C. Catto, S. Bernardini, T. Fiorido, K. Aguir, E. Longo, V.R. Mastelaro, L.F. da Silva, M.P.F. de Godoy, Highly selective ozone gas sensor based on nanocrystalline $Zn_{0.95}Co_{0.05}O$ thin film obtained via spray pyrolysis technique, Appl. Surf. Sci. 418 (2019) 347.

[59] A.C. Catto, L.F. da Silva, M.I.B. Bernardi, S. Bernardini, K. Aguir, E. Longo, V.R. Mastelaro, Local structure and surface properties of $Co_xZn_{1-x}O$ thin films for ozone gas sensing, ACS Appl. Mater. Interfaces 8 (2016) 26066.

[60] A.C. Catto, L.F. da Silva, C. Ribeiro, S. Bernardini, K. Aguir, E. Longo, V.R. Mastelaro, An easy method of preparing ozone gas sensors based on ZnO nanorods, RSC Adv. 5 (2015) 19528.

[61] L.F. da Silva, J.-C.M'Peko, A.C. Catto, S. Bernardini, V.R. Mastelaro, K. Aguir, C. Ribeiro, E. Longo, UV-enhanced ozone gas sensing response of $ZnO-SnO_2$ heterojunctions at room temperature, Sensors Actuators B Chem. 240 (2017) 573.

[62] S. Thirumalairajan, V.R. Mastelaro, A novel organic pollutants gas sensing material p-type $CuAlO_2$ microsphere constituted of nanoparticles for environmental remediation, Sens. Actuators B 223 (2016) 138.

[63] L.F. da Silva, V.R. Mastelaro, A.C. Catto, C.A. Escanhoela, S. Bernardini, S.C. Zilio,E. Longo, K. Aguir, Ozone and nitrogen dioxide gas sensor based on a nanostructured SrTi0.85Fe0.15O3 thin film, J. Alloys Compd. 638 (2015) 374.

**Figure and table captions**

**Fig. 1**: (a) Shape of $In_2S_3$ film, (b) Ozone detection experimental set-up.

**Fig. 2(a)**: GIXD pattern of $In_2S_3$ film for different X-ray incidence angles.

**Fig. 2(b)**: Williamson-Hall plot for $In_2S_3$ film.

**Fig. 3**: (a) 2D AFM topographic image of $In_2S_3$ film, (b) 3D AFM topographic image, (c) SEM topographic images and (d) grain size distribution.

**Fig. 4**: EDS spectra: (a) $In_2S_3$ film and (b) glass substrate.

**Fig. 5:** XPS spectra of $In_2S_3$ film: (a) survey spectrum, (b) S 2p, (c) In 3d and (d) O 1s.

**Fig. 6**: Optical properties of $In_2S_3$ film. (a) derivative of transmittance with respect to wavelength, inset shows optical transmission and total reflection, (b) plot of $ln(\alpha h v)$ vs. $ln(h v - E_g)$, (c) variation of $(\alpha h v)^2$ vs. photon energy, and (d) PL spectrum for $\lambda_{exc} = 400$ nm.

**Fig. 7**: (a) Resistance change of the $In_2S_3$ sensor exposed to 400 ppb of ozone at 200°C, (b) dynamic change in the resistance of a thin film of $In_2S_3$ during interaction with 400 ppb of $O_3$ at several working temperatures, (c) evolution of sensor response to ozone ($R_{ozone}/R_{air}$) and ($R_{air}/R_{nitrogen}$) vs. operating temperature, (d) Resistance change of $In_2S_3$ sensor exposed to air and nitrogen at different operating temperature.

**Fig. 8**: Dynamic change in resistance and response of a thin film of $In_2S_3$ exposed to several concentrations of $O_3$ at a working temperature of 160°C, (b) response vs. ozone concentration, (c) response and recovery times vs. ozone concentration (d) repeatability of the $In_2S_3$ sensor exposed to 125 ppb of ozone at 160° C.

**Fig. 9**: Selectivity of $In_2S_3$ sensor at working temperatures of 160°C and 350°C.

**Table 1:** Atomic concentrations of constituent elements of $In_2S_3$ film deposited on glass substrate.

**Table 2:** Sensing performances of the developed $In_2S_3$ ozone sensor compared with those previously published.
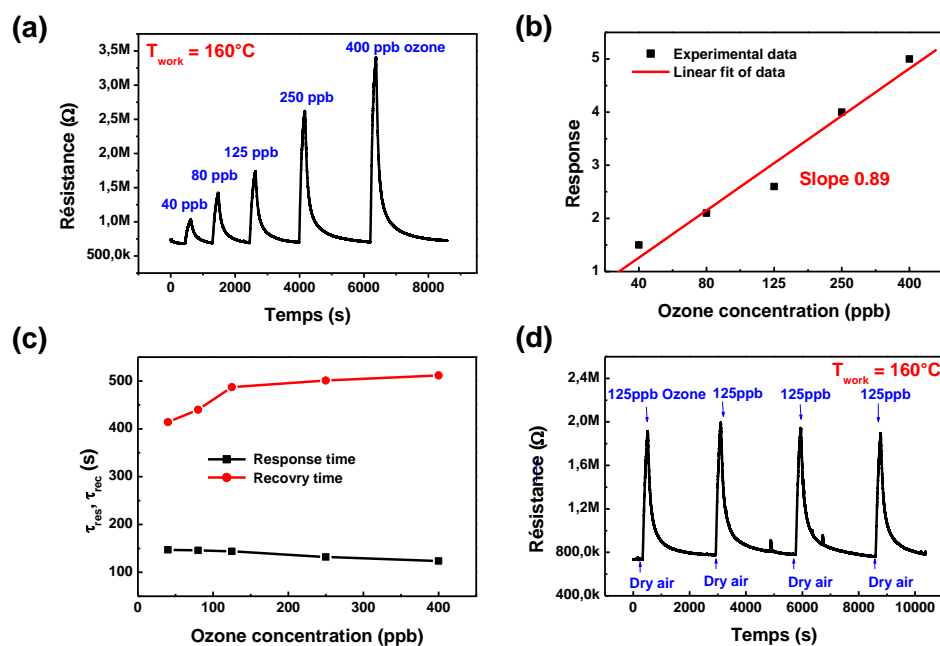
(a) *Dynamic change in resistance and response of a thin film of $In_2S_3$ exposed to several concentrations of $O_3$ at a working temperature of 160°C, (b) response vs. ozone concentration, (c) response and recovery times vs. ozone concentration (d) repeatability of the $In_2S_3$ sensor exposed to 125 ppb of ozone at 160° C.*

.

**Highlights**

- $In_2S_3$ films deposited by spray pyrolysis technique on $SiO_2/Si$ substrates show good sensitivity towards ozone gas.

- Sensing response versus working temperature reveals an optimal temperature of 160°C.

- Response and recovery times for 40 ppb $O_3$ are 147 s and 414 s respectively at optimum temperature.

- The response of the $In_2S_3$ sensor increases from 1.5 to 5 by varying $O_3$ concentration from 40 ppb to 400 ppb at 160°C.

- $In_2S_3$ sensor is highly sensitive to ozone and nitrogen dioxide at 160°C while at 350°C this property is balanced in favor of volatile organic compounds.

Table 1

Table 1

| Element | C | O | Na | Mg | Al | Si | S | Cl | K | Ca | In |
|---------|------|------|------|------|------|-------|------|------|------|------|------|
| Weight% | 8.86 | 28.7 | 6.70 | 1.93 | 0.6 | 35.11 | 3.41 | 1 | 0.45 | 6.1 | 7.13 |
| Atomic% | 16.27 | 39.56 | 6.42 | 1.75 | 0.49 | 27.56 | 2.35 | 0.62 | 0.25 | 3.36 | 1.37 |

Table 2

Click here to access/download;Table;Table 2.docx ⬇

**Table 2**

| Material | LOD (ppb) | T (°C) | Response | $\tau_{rep}$ / $\tau_{rec}$ (s) | Year | Ref |
|---|---|---|---|---|---|---|
| $\beta$-$In_2S_3$ | 40 | 160 | $1.5^a$ | 147/414 | 2021 | This work |
| Hierarchicalbranch-like$In_2O_3$ | 200 | 70 | $5^a$ | -/- | 2021 | [54] |
| $ZnCo_2O_4$ microspheres | 80 | 200 | $0.23^b$ | 8 /10 | 2018 | [57] |
| $Zn_{0.95}Co_{0.05}$ O | 20 | 250 | $0.4^b$ | 46/62 | 2019 | [58] |
| $Zn_{0.95}Co_{0.05}$ O | 42 | 200 | $5^b$ | 40/360 | 2016 | [59] |
| ZnO | 60 | 250 | $3^a$ | 9/300 | 2015 | [60] |
| $ZnO$-$SnO_2$ | 20 | RT(UV) | $8^a$ | -/- | 2017 | [61] |
| $CuAlO_2$ | 200 | 200 | $1.9^a$ | 29/45 | 2016 | [62] |
| $SrTi_{0.85}Fe_{0.15}O_3$ | 100 | 260 | $3^a$ | 26/72 | 2015 | [63] |

$^a$ :Response = $R_{gas}/R_{air}$

$^b$ :Response = $(R_{gas} - R_{air})/R_{air}$

Figure 1

Figure 1

Figure 2(a)

Click here to access/download;Figure;Fig. 2(a).TIF ⬇

Figure 2(b)

Figure 4

Figure 5

Click here to access/download;Figure;Fig. 5.tif

Figure 6

Click here to access/download;Figure;Fig. 6.TIF ⬇

Figure 7

Click here to access/download;Figure;Fig. 7.TIF ±
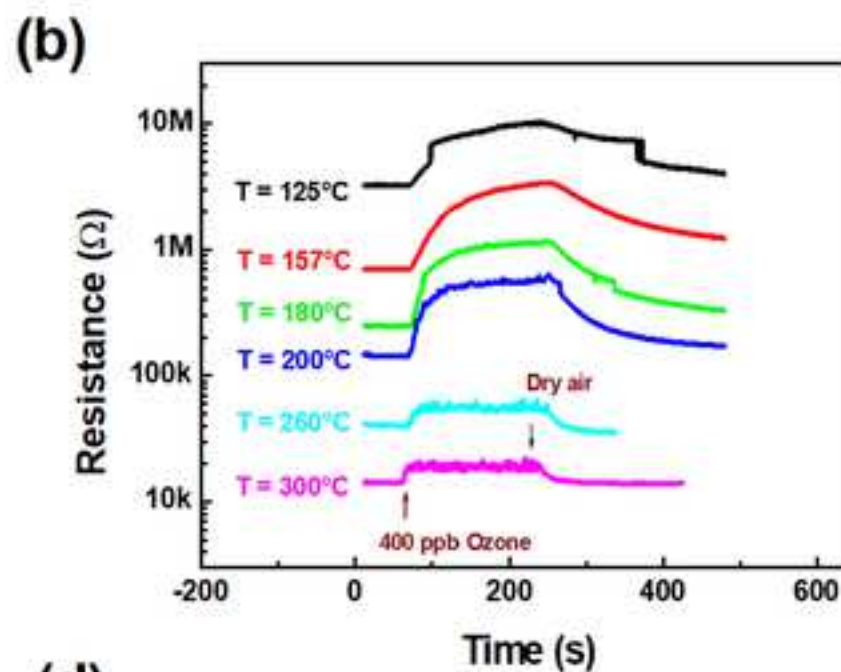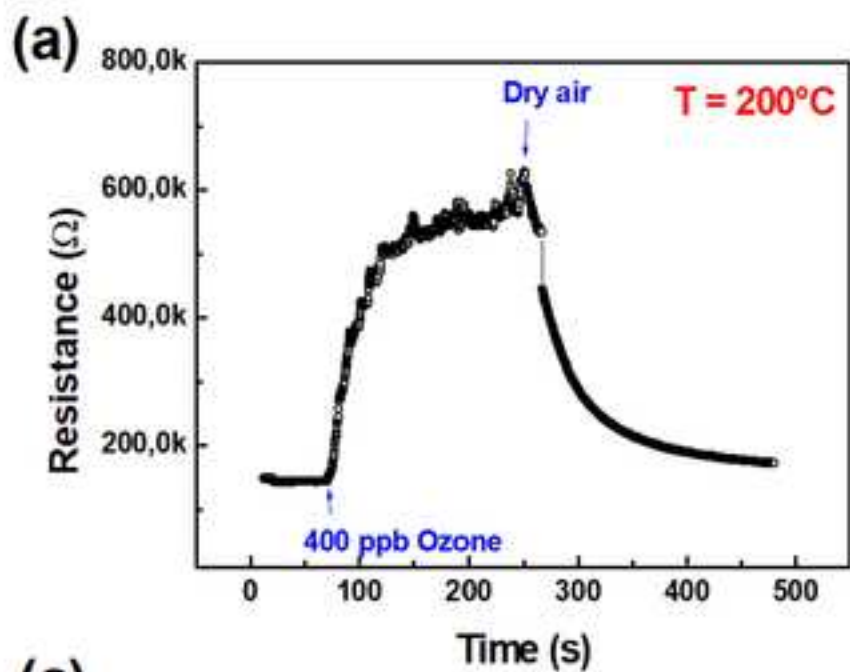
Figure 8

Figure 9

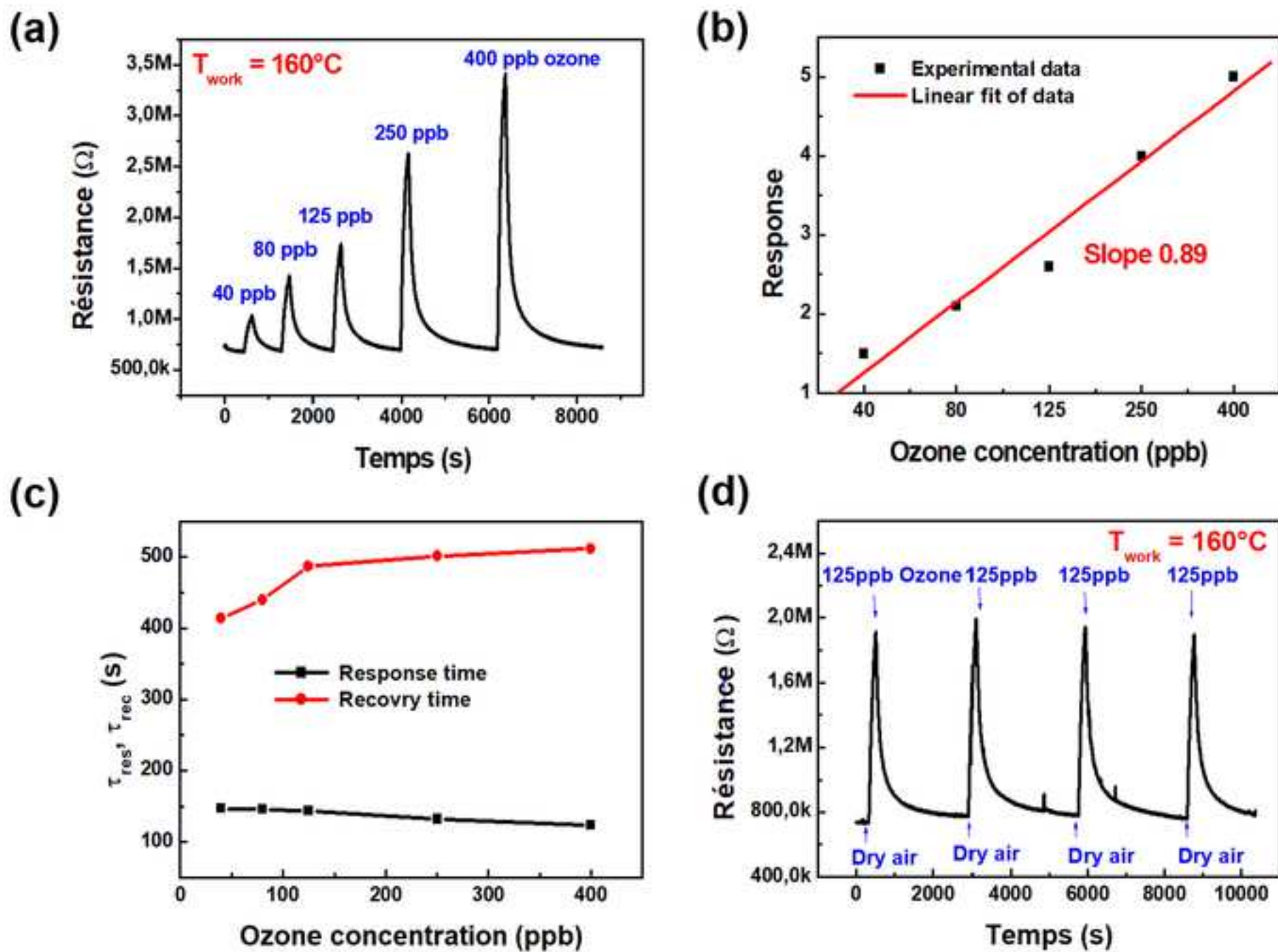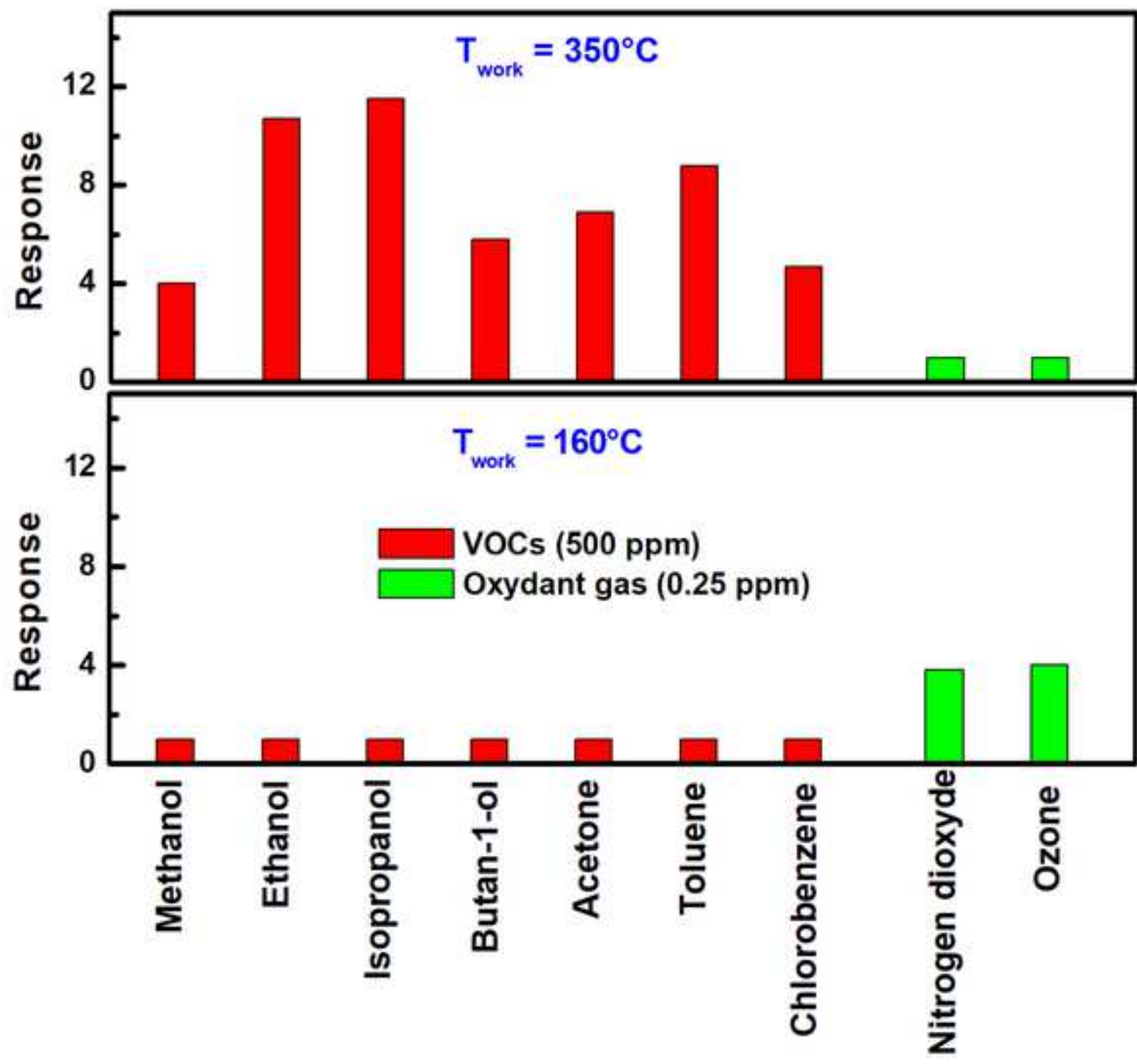Click here to access/download;Figure;Fig. 9.TIF ⬇
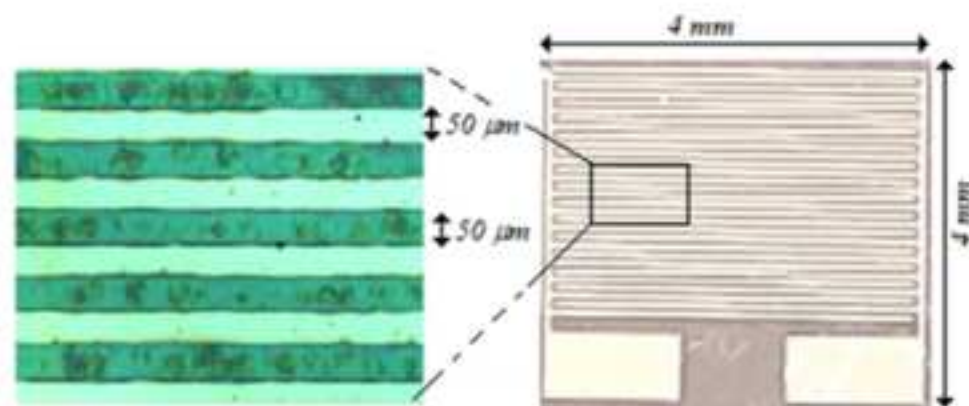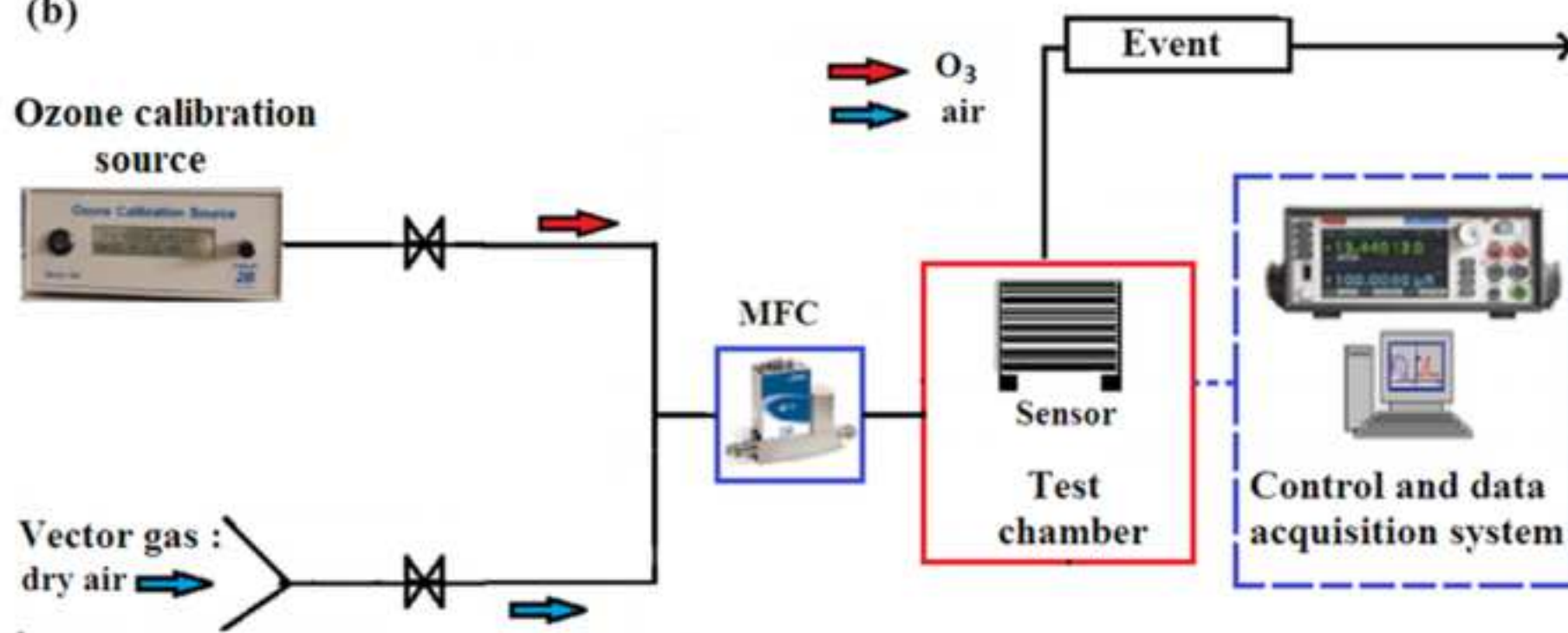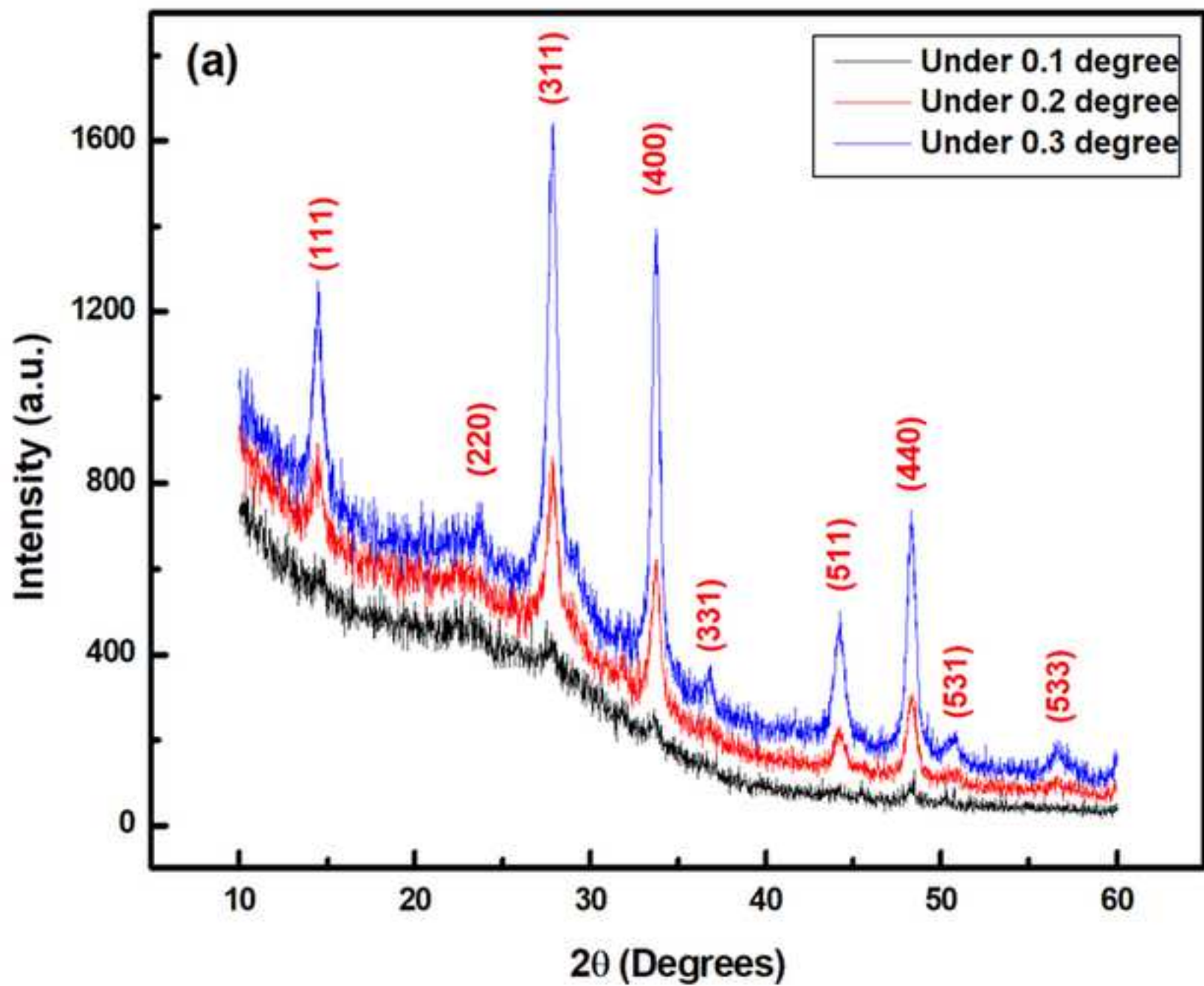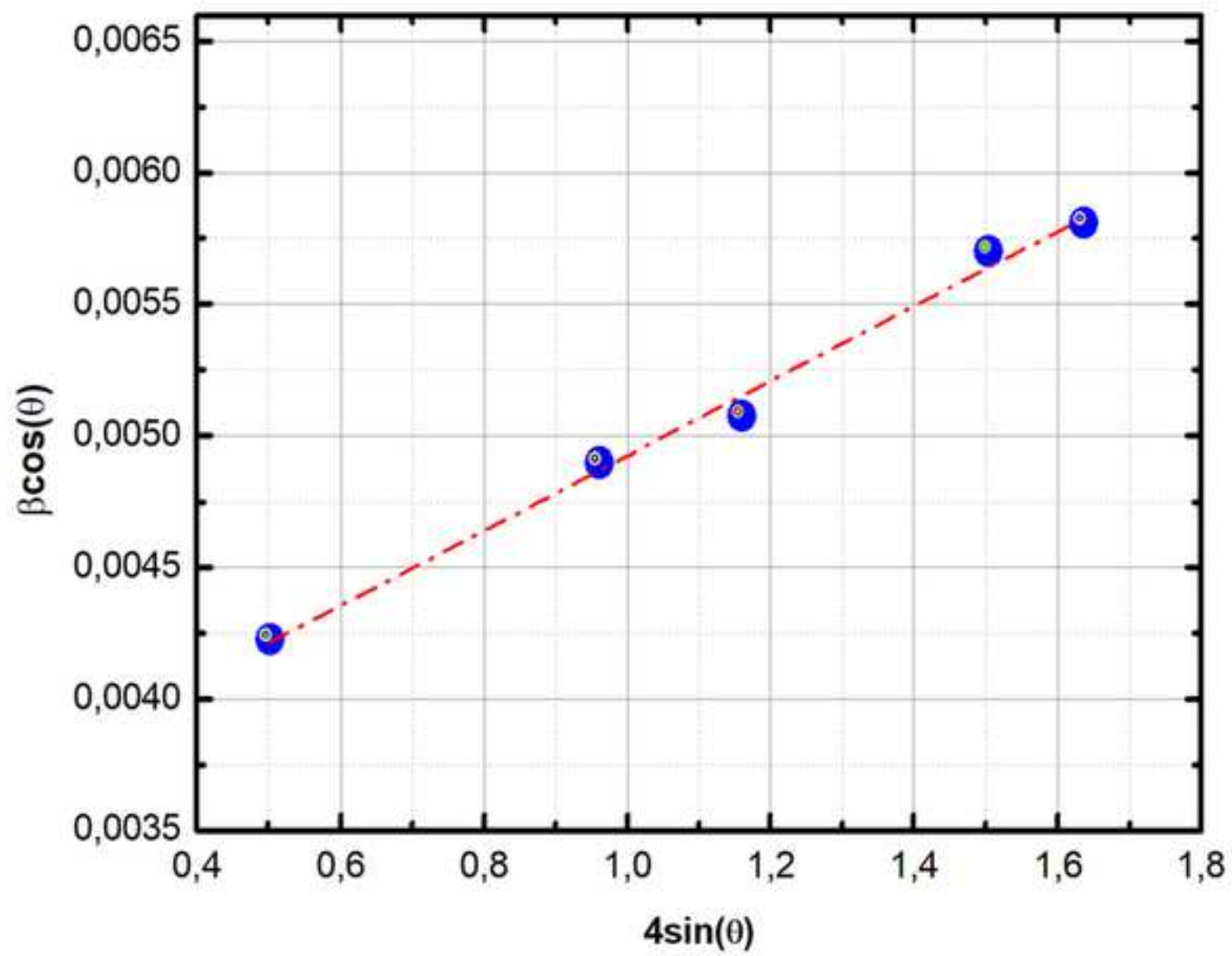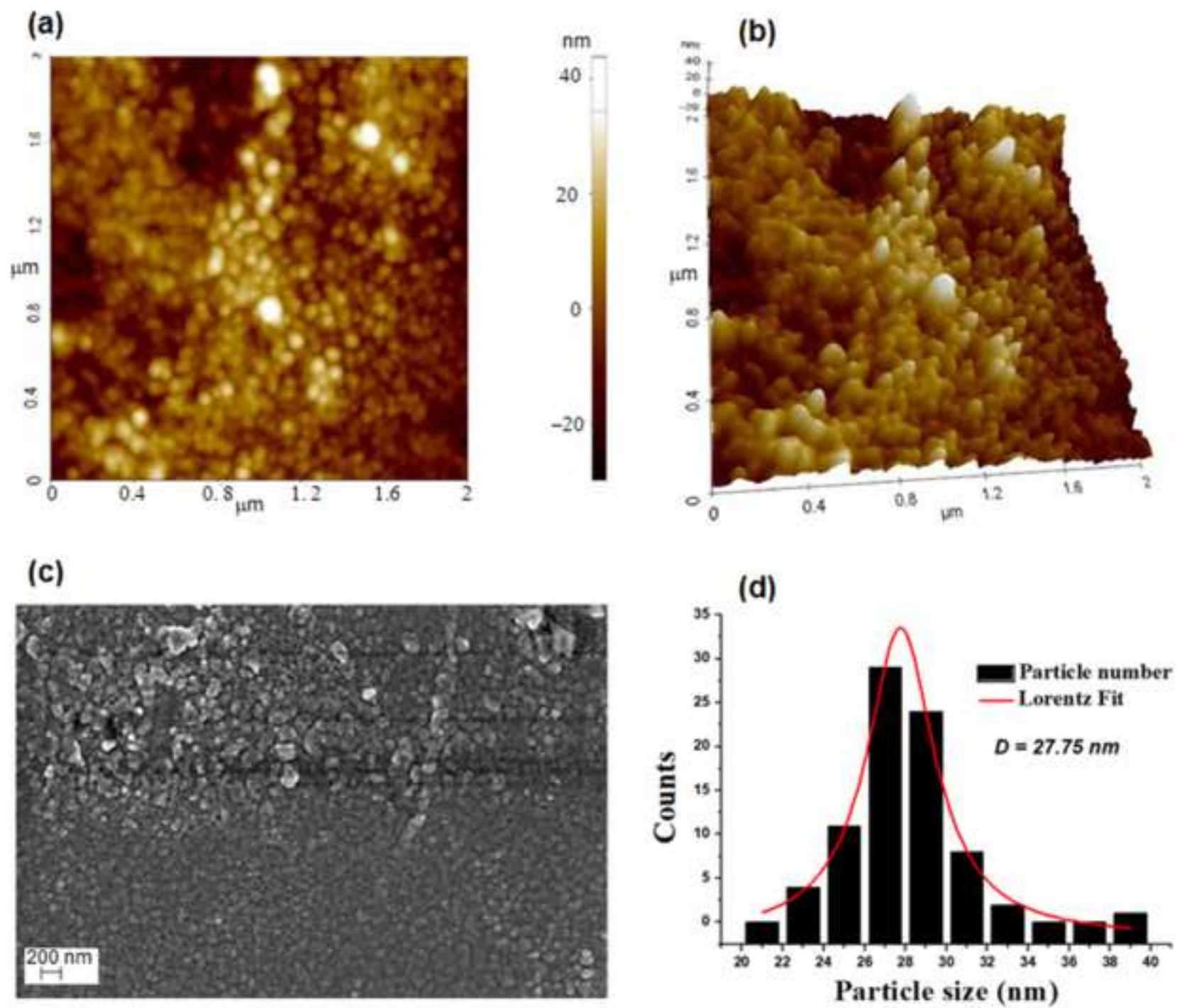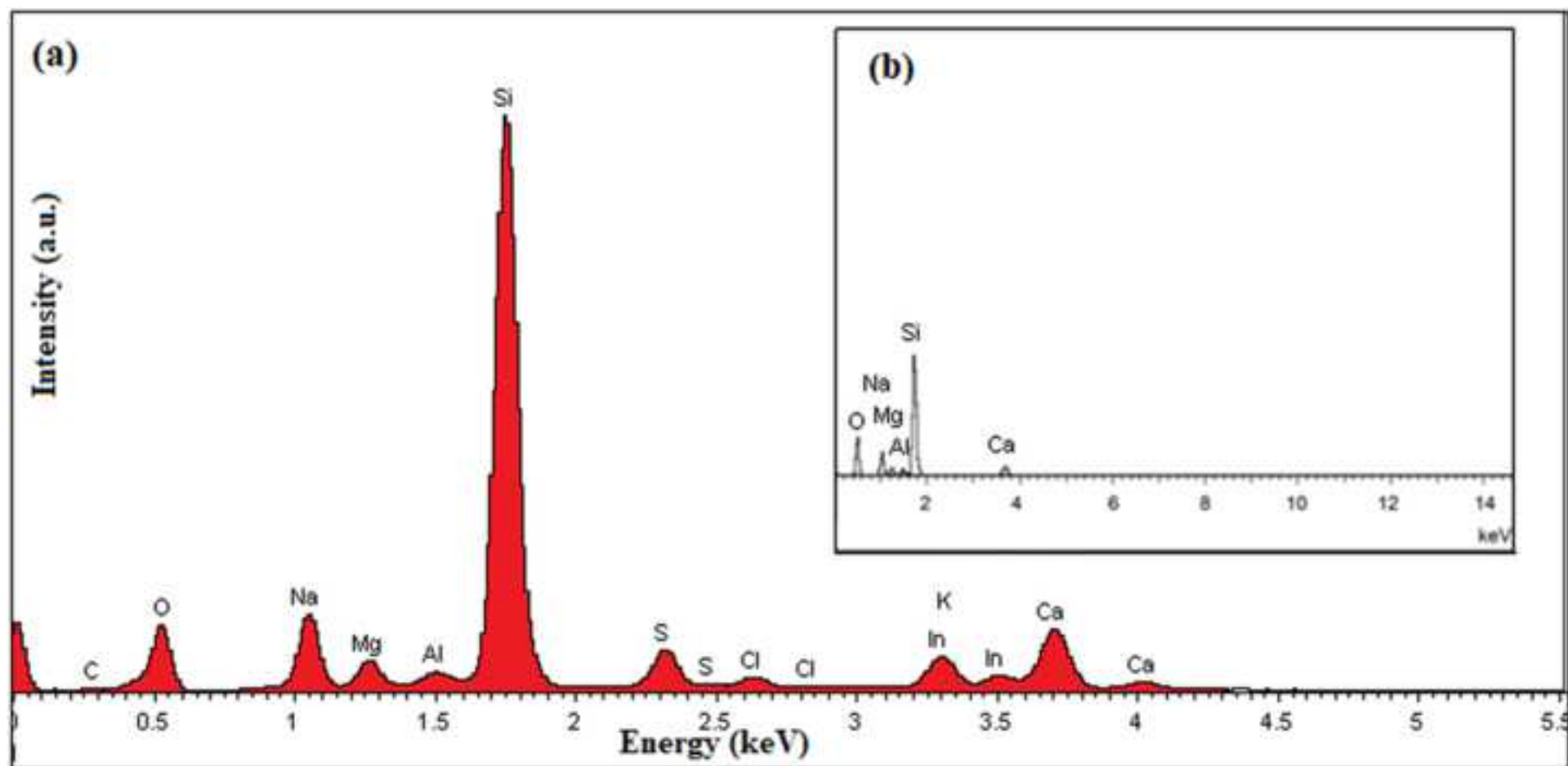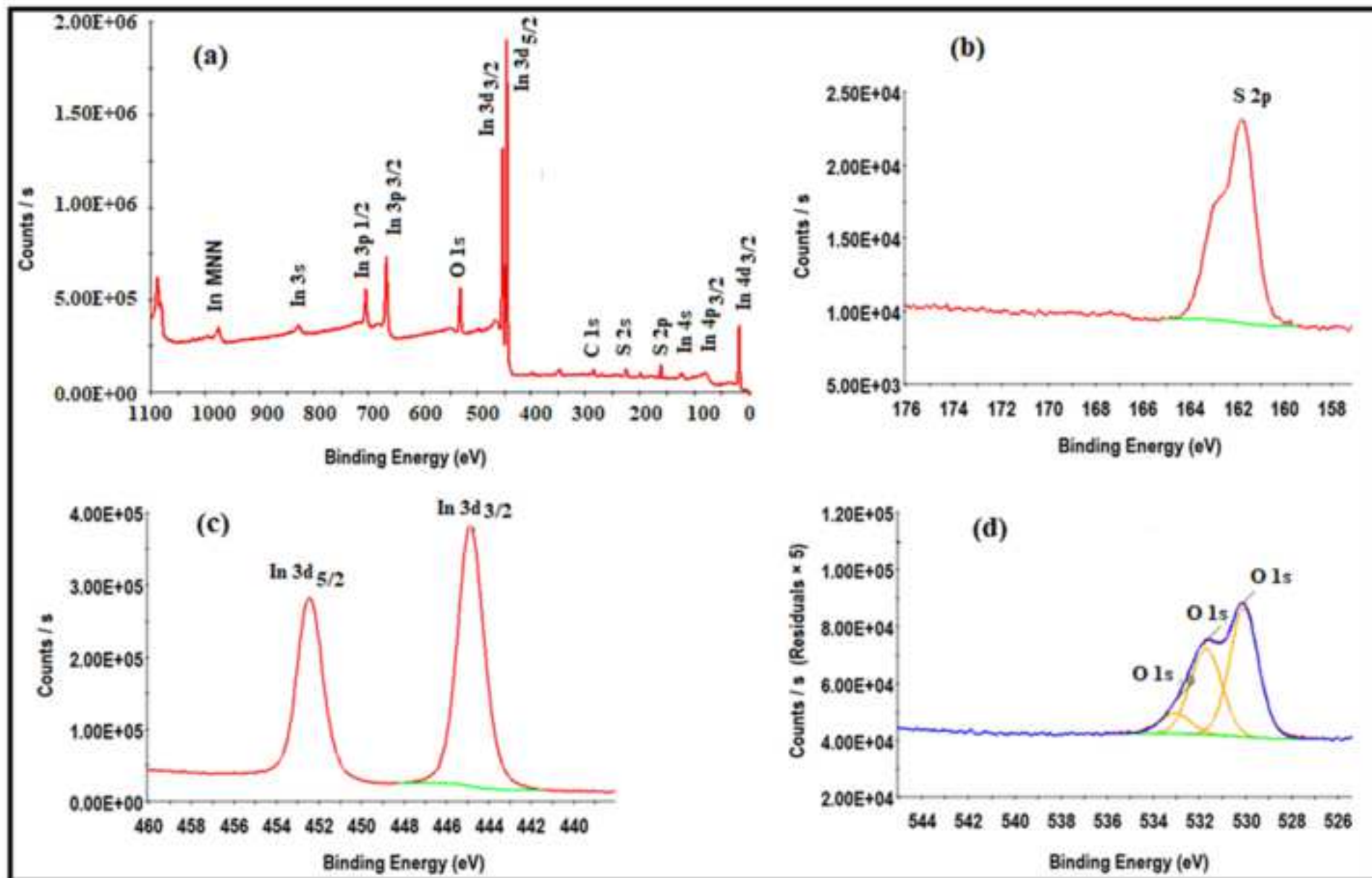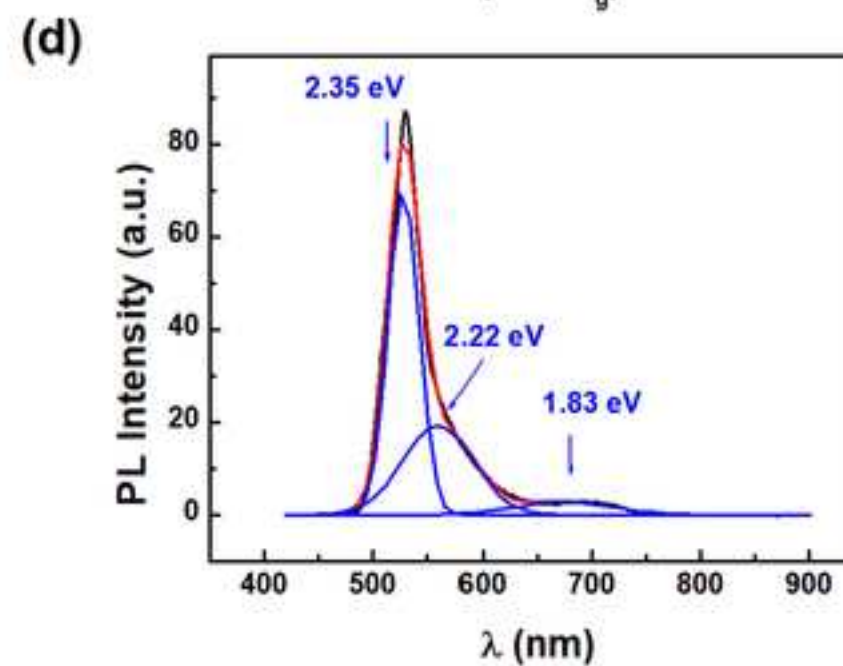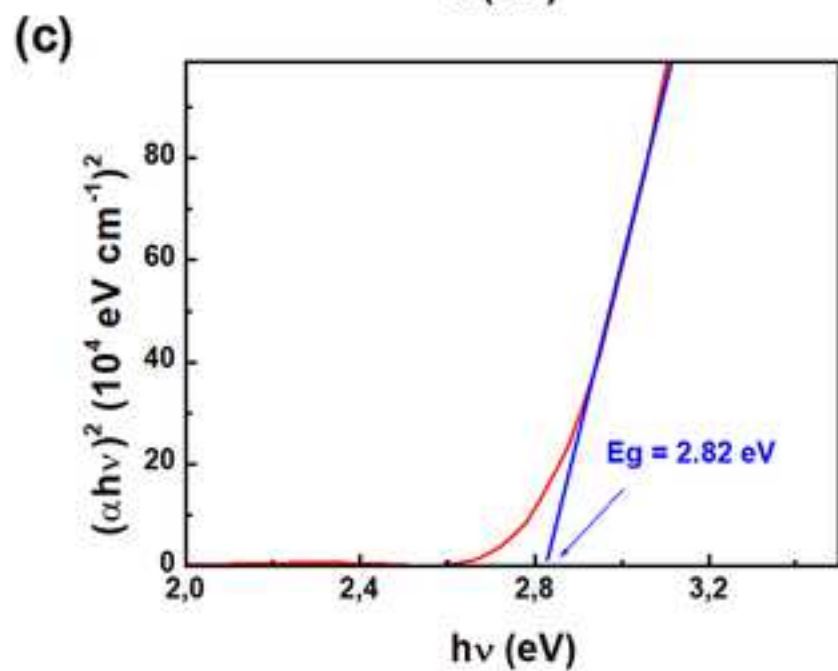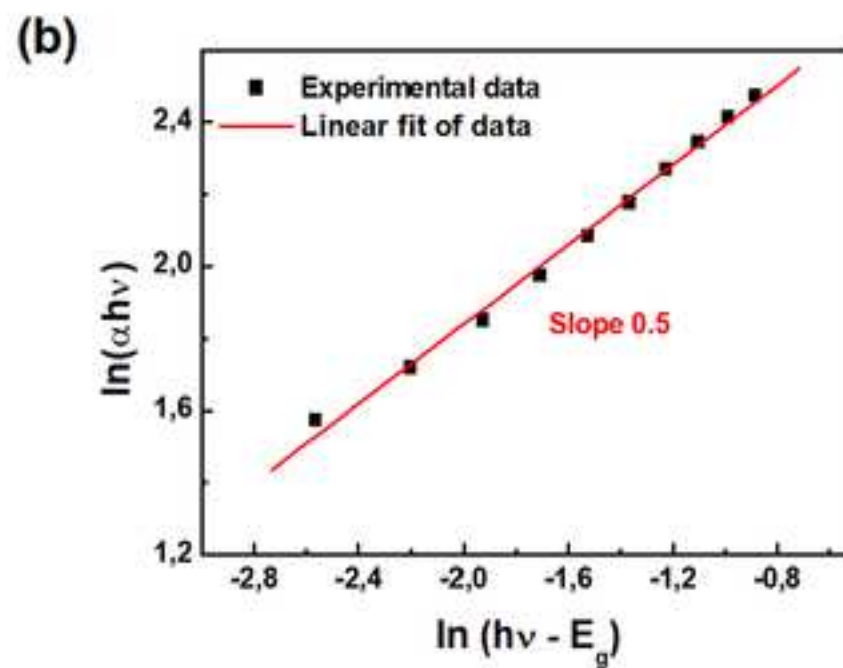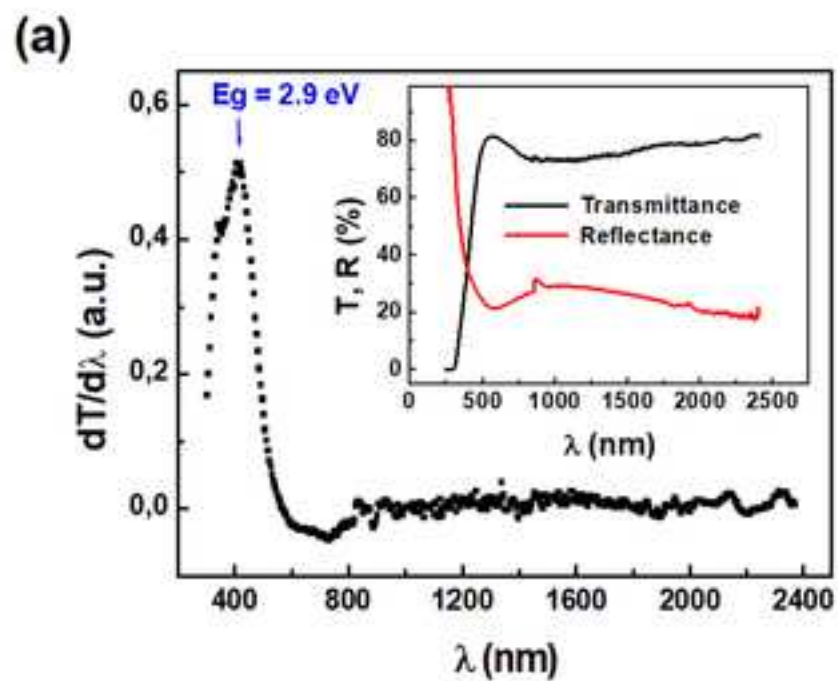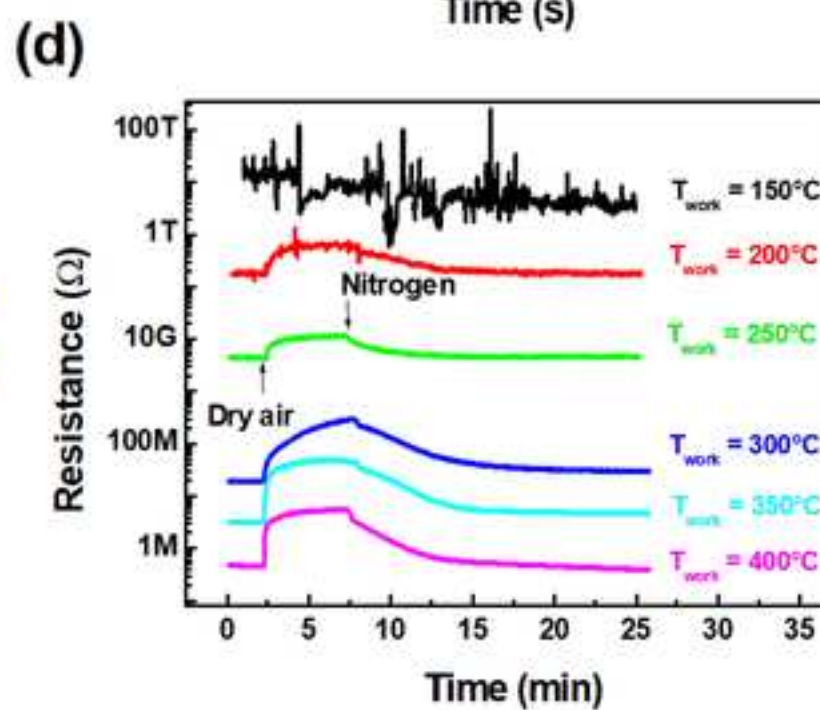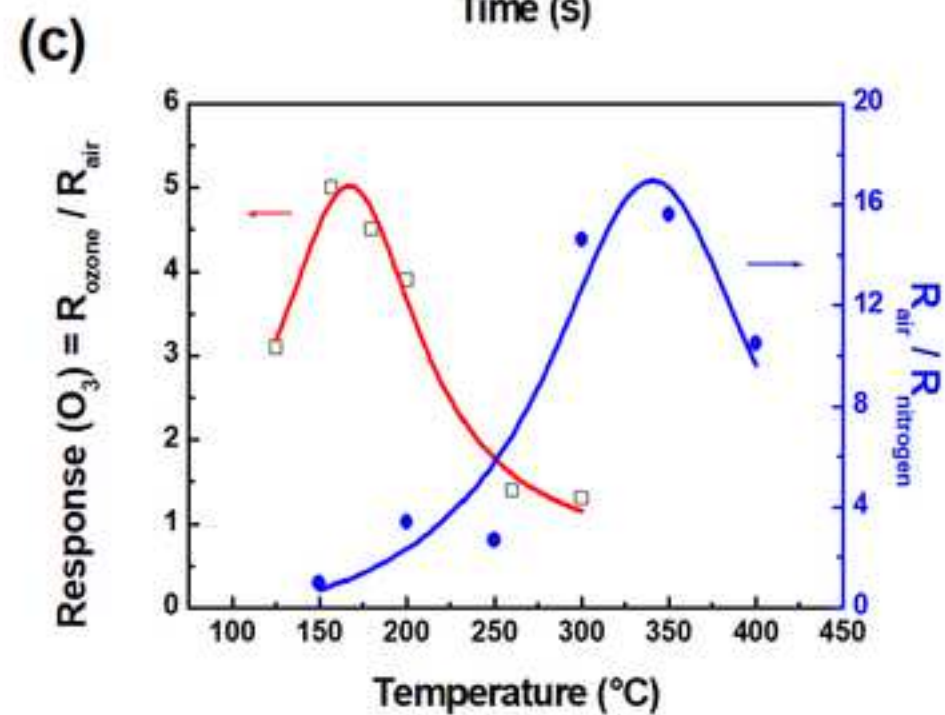
**Declaration of competing interest**

☒The authors declare that they have no known competing financial interests or personal relationships that could have appeared to influence the work reported in this paper. ☐The authors declare the following financial interests/personal relationships which may be considered as potential competing interests.